Research Article

Modeling compressive strength of Moroccan fly ash–phosphogypsum geopolymer bricks

Mohamed Vadel Bebana[1] · Khadija Ziat[1] · Nawal Semlal[2] · Mohamed Saidi[1]

Received: 9 July 2019 / Accepted: 20 November 2019 / Published online: 25 November 2019

Abstract
Fly ash and phosphogypsum are industrial by-products requiring a cost to get rid of. Their potential use in the synthesis of geopolymer bricks provides great benefits such as the saving use of natural resources and the solid by-product waste management. Compressive strength is the most important parameter for geopolymer bricks design. In this study, two artificial neural networks, namely the multilayer perceptron (MLP) and the radial basis function (RBF) networks, have been investigated to predict the compressive strength. While developing the MLP or RBF models, 99 experimental observations were used for training and testing. Two evaluation steps were performed: The first step determined the effective number of hidden layers and neurons in each hidden layer as well as the appropriate activation function in predicting the compressive strength. The second evaluation step evaluated the accuracy with which the model would predict the compressive strength of geopolymers. The MLP neural network with two hidden layers having 8 and 10 neurons and the hyperbolic tangent activation function was the best model for predicting the compressive strength. Artificial neural networks can be used as a reliable and accurate technique for estimating the parameters of geopolymer materials.

Keywords Phosphogypsum · Fly ash · Geopolymer bricks · Modeling

List of symbols

$\bar{y}_{prd}$	Mean of predicted values
β	Weight vector connecting the hidden neurons to the output neuron
σ	Impact factor of radial basis function
a_j	Weight vector connecting the jth hidden neuron
b_j	Threshold of the jth hidden neuron
c	Center of radial basis function
f	Output function
g	Activation function
N	Number of hidden neurons
n	Number of experimental data
R^2	Coefficient of determination
x_i	Vector of the ith input neuron
y_{exp}	Experimental values
y_{prd}	Predicted values

Abbreviations

ANN	Artificial neural network
AT	Aging time
BP	Back-propagation
CS	Compressive strength (MPa)
CT	Curing temperature (°C)
FA	Fly ash
LM	Levenberg–Marquardt
MAE	Mean absolute of errors
MLP	Multilayer perceptron
PFA	Percentage of fly ash
PG	Phosphogypsum
PPG	Percentage of phosphogypsum
RBF	Radial basis function
RMSE	Root mean square errors
SHC	Sodium hydroxide concentration
W	Water

✉ Khadija Ziat, khadijaziat@gmail.com | [1]Laboratoire Physico-Chimie des Matériaux, Substances Naturelles et Environnement, Faculty of Sciences and Techniques, Abdelmalek Essaâdi University, Tangier, Morocco. [2]OCP S.A, Jorf Lasfar, Morocco.

1 Introduction

Dumping or landfilling the solid by-product has a negative impact on the environment leading to many types of pollution. Therefore, the urgent investigation of the reuse of by-products is fundamental ensuring new materials to be safely and efficiently used in different applications. Fly ash (FA) is a solid waste generated from coal-fired electric power stations. The by-product phosphogypsum (PG) is obtained during the wet process phosphoric acid production by attacking phosphate rock by sulfuric acid. Many researchers have valorized these materials by their incorporating as a binder in cementitious materials [1–4]. Altun and Sert [1] reported that phosphogypsum can be used in place of natural gypsum for Portland cement. The authors found that 3 wt% PG is the optimal content showing the highest mechanical property. Shen et al. [2] studied the effect of incorporating PG to improve the performances of lime–FA binder. The results showed that phosphogypsum promotes the binder action between lime and fly ash. Kumar [3] investigated the production of bricks from fly ash–lime–phosphogypsum. Outcomes indicate that these bricks are comparable with those of the ordinary burnt clay. Moreover, they are lighter and could be used for building construction. Shen et al. [4] reported that phosphogypsum can be used to produce the calcium sulfoaluminate cement with an optimal firing temperature between 1250 and 1300 °C.

Geopolymers, originally proposed by the French scientist Davidovits [5], designated a large range of materials characterized by chains or networks of inorganic molecules that can be used as a binder in concrete. Their main properties are quick compressive strength development, low permeability, resistance to acid attack and good resistance to freezing cycles [6]. The geopolymers were produced from a vast variety of raw materials such as metakaolin [7], clay [8] and other natural silica-aluminates [9] as well as industrial process wastes such as coal fly ash [10, 11], lignite bottom ash [12], metallurgical slag [13, 14] and phosphogypsum [15, 16].

The prediction of the compressive strength is an essential parameter for successful geopolymer design. Indeed, several researchers have predicted the compressive strength using different methods such as the regression analysis, the genetic algorithm, the fuzzy logic and the artificial neural networks [17–20]. ANN is one of the most commonly applied methods because of its effectiveness and large applicability [21–23]. Nazari and Torgal [24] have developed different models based on ANNs to predict the compressive strength of various types of geopolymers. Mansour et al. [25] built trained and tested ANNs to predict the ultimate shear strength of reinforced concrete beams with transverse reinforcements. Recently, Naderpour et al. [26] have predicted the compressive strength of recycled aggregate concrete using artificial neural networks.

The present study aims the prediction of the compressive strength of Moroccan fly ash–phosphogypsum geopolymer bricks by using radial basis function and multilayer perceptron neural networks. The effects of the number of hidden layers, the neurons in hidden layers as well as the activation functions on the prediction of the compressive strength were evaluated. Various input parameters of models are considered, whereas the compressive strength is used independently as the output parameter.

2 Materials and methods

2.1 Materials and sample preparation

Fly ash used in this study was from LafargeHolcim in the west of Morocco. Phosphogypsum is issued from phosphate rock original from Morocco. FA was used in its natural particle size distribution without further reduction through milling. PG was washed with tap water, filtered and dried in the oven at 60 °C for 24 h, then grounded and sieved through a sieve of 120 µm. Figure 1 shows the materials used for making geopolymer bricks at a laboratory scale. The chemical compositions of fly ash and phosphogypsum are shown in Table 1.

The sodium hydroxide NaOH (analytical reagent grade, Fluka) solution was obtained by dissolving sodium hydroxide pellets in bi-distilled water and allowed to cool to room temperature. The mixtures were obtained by hand mixing for 5 min.

Samples were prepared from fly ash, washed and sieved phosphogypsum, alkaline liquid and tap water. FA was partially replaced with PG at the level of, 0, 5, 10, 15, 20, 25 and 30% by weight. Four concentrations of NaOH 1, 5, 10 and 15 M were added to a different liquid ratio to form geopolymer pastes. The paste samples were cast in cylindrical plastic molds with a diameter of 20 mm and height of 30 mm and vibrated to remove entrapped air. The manufacturing process of FA–PG-based geopolymer bricks is shown in Fig. 2. The specimens were cured at a temperature of 60, 80 and 100 °C for 24 h in order to accelerate the geopolymer reaction and thus achieve the hardening of the structure. The bricks were placed in room temperature until the aging time test which was 3, 7 or 28 days.

Fig. 1 Materials

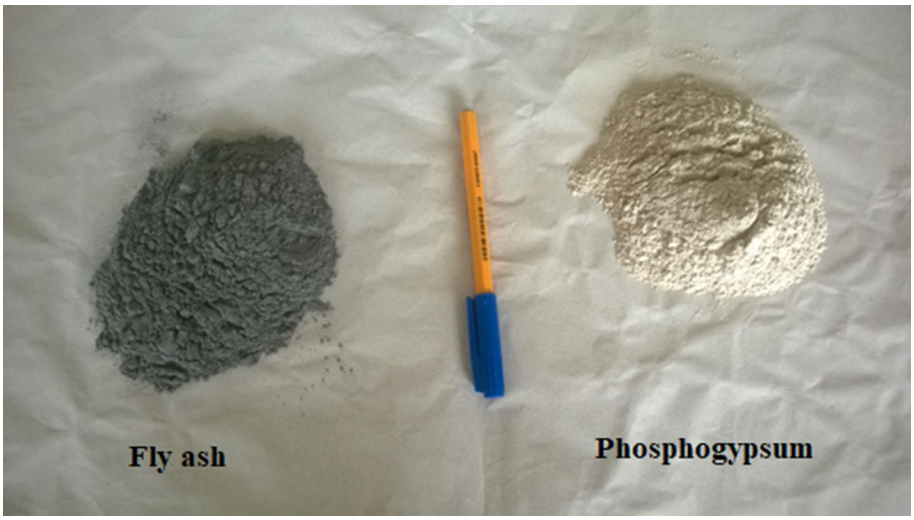

Table 1 Chemical composition of fly ash and phosphogypsum in weight percentage of oxides

Composition (%)	SiO_2	Al_2O_3	Fe_2O_3	CaO	MgO	SO_3	P_2O_5	F	LOI
FA	50.85	26.55	3.69	5.45	1.56	0.46	1.16	–	6.89
PG	2.06	1.04	4.28	20	0.137	43.5	0.697	2.48	22

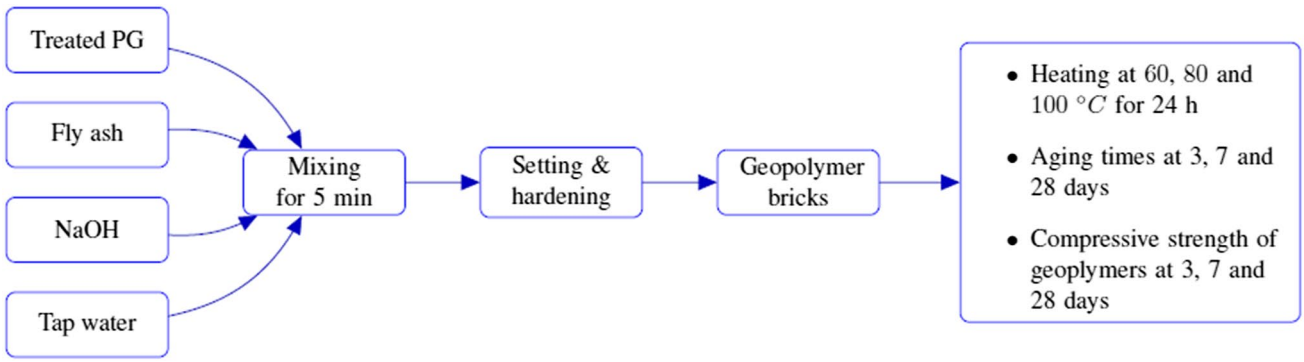

Fig. 2 Flowchart of the experimental procedure of FA–PG geopolymer bricks synthesis

2.2 Compressive strength test

The compressive strengths of specimens at 3, 7 and 28 days were determined following the procedure described in BS EN 1961:2005 using an automatic compression test machine. Four compression strength tests were carried out for samples prepared with each ratio, and the values reported were the averages of the four compression strength values. Table 2 shows the details of the mixture proportions and the corresponding results under the considering experimental conditions. The specimens that contain FA, PG and NaOH solutions are abbreviated as FAPG1 to FAPG33.

2.3 Artificial neural network and performance of models

The artificial neural network is a system of data processing based on the working mechanism of the brain. The fundamental processing consists of a linear combination of input variables into a hidden layer of units where new combinations are created as final output variables. The architecture of ANN requires the knowledge of the number of network layers, the number of neurons in the layers as well as the learning algorithms and the neuron transfer functions. The theoretical backgrounds of neural network models can be found in [27–31].

Table 2 Details of mix proportions for different FA–PG-based geopolymer bricks

Samples	FA (%)	PG (%)	NaOH (M)	Added water (%)	Water solid ratio	Aging time (days)	Temperature (°C)
FAPG1	100	0	1	39.6	0.396	3, 7, 28	60
FAPG2	95	5	1	39.1	0.391	3, 7, 28	60
FAPG3	90	10	1	38.6	0.386	3, 7, 28	60
FAPG4	85	15	1	38.1	0.381	3, 7, 28	60
FAPG5	80	20	1	37.6	0.376	3, 7, 28	60
FAPG6	75	25	1	37.1	0.371	3, 7, 28	60
FAPG7	70	30	1	36.6	0.366	3, 7, 28	60
FAPG8	100	0	1	39.6	0.396	3, 7, 28	80
FAPG9	95	5	1	39.1	0.391	3, 7, 28	80
FAPG 10	90	10	1	38.6	0.386	3, 7, 28	80
FAPG 11	85	15	1	38.1	0.381	3, 7, 28	80
FAPG 12	80	20	1	37.6	0.376	3, 7, 28	80
FAPG 13	75	25	1	37.1	0.371	3, 7, 28	80
FAPG 14	70	30	1	36.6	0.366	3, 7, 28	80
FAPG 15	100	0	1	39.6	0.396	3, 7, 28	100
FAPG 16	95	5	1	39.1	0.391	3, 7, 28	100
FAPG 17	90	10	1	38.6	0.386	3, 7, 28	100
FAPG 18	85	15	1	38.1	0.381	3, 7, 28	100
FAPG 19	80	20	1	37.6	0.376	3, 7, 28	100
FAPG 20	75	25	1	37.1	0.371	3, 7, 28	100
FAPG 21	70	30	1	36.6	0.366	3, 7, 28	100
FAPG 22	80	20	1	39.6	0.396	3, 7, 28	60
FAPG 23	80	20	1	39.4	0.394	3, 7, 28	60
FAPG 24	80	20	1	39.2	0.392	3, 7, 28	60
FAPG 25	80	20	5	38	0.38	3, 7, 28	60
FAPG 26	80	20	5	37	0.37	3, 7, 28	60
FAPG 27	80	20	5	36	0.36	3, 7, 28	60
FAPG 28	80	20	10	35.5	0.355	3, 7, 28	60
FAPG 29	80	20	10	34	0.34	3, 7, 28	60
FAPG 30	80	20	10	32	0.32	3, 7, 28	60
FAPG 31	80	20	15	33.5	0.335	3, 7, 28	60
FAPG 32	80	20	15	31	0.31	3, 7, 28	60
FAPG 33	80	20	15	28	0.28	3, 7, 28	60

The radial basis function network applies RBF neurons in its hidden layer. Each RBF node is composed of a centroid, an impact factor, and its output is a function with radial symmetry [27, 28].

The multilayer perceptron is a class of feedforward neural network that has been commonly used for the approximate function [28]. The MLP learns the information of the dataset pattern using an algorithm known as "training." This algorithm modifies the weights of the neurons according to the error between the values of real output and target output, where it provides nonlinear regression between the input variables and the output variables [32]. The back-propagation (BP) with the gradient descent technique and Levenberg–Marquardt (LM) is

Table 3 Used activation functions and output functions

ANN type	Output function	Activation function
RBF [27]	$f(x) = \sum_{i=1}^{N} \beta_i g_i(x)$	$g_i(x) = \exp\left(-\frac{\|x-c_i\|^2}{2\sigma_i^2}\right)$
MLP [28]	$f(x) = \sum_{j=1}^{N} \beta_j g\left(\sum_{i=1}^{n} a_j x_i + b_j\right)$	$g(x) = \frac{e^{2x}-1}{e^{2x}+1}$ $g(x) = \frac{1}{1+e^{-x}}$

c_i and σ_i are the center and impact factor of the ith RBF node, x is the input vector, and $\|.\|$ denotes a norm that is usually Euclidean. β_i is the weight connecting the ith RBF hidden node to the output node, and g is the activation function. a_j is the weight vector connecting the jth hidden neuron and the input neurons, and b_j is the threshold of the jth hidden neuron. $a_j x_i$ represents the inner product of a_j and x_i, N is the number of hidden neurons, and n is the number of experimental data

the most well-known training algorithms for the multilayer perceptron [32]. Table 3 lists the output functions of the RBF and MLP network models and the used activation functions.

To evaluate the performances of models, three error functions, namely the coefficient of determination (R^2) [33], the root mean square error (RMSE) and the mean absolute error (MAE) [34], are used. Their mathematical expressions are as follows:

$$R^2 = \frac{\sum_{i=1}^{n} \left(y_{\text{exp},i} - \bar{y}_{\text{prd}}\right)^2}{\sum_{i=1}^{n} \left(y_{\text{exp},i} - \bar{y}_{\text{prd}}\right)^2 + \sum_{i=1}^{n} \left(y_{\text{exp},i} - y_{\text{prd},i}\right)^2} \quad (1)$$

$$\text{RMSE} = \sqrt{\frac{1}{n} \sum_{i=1}^{n} \left(y_{\text{exp},i} - y_{\text{prd},i}\right)^2} \quad (2)$$

$$\text{MAE} = \frac{1}{n} \sum_{i=1}^{n} \left| \left(y_{\text{exp},i} - y_{\text{prd},i}\right) \right| \quad (3)$$

where y_{exp} and y_{prd} are the experimental and predicted output values and $\bar{y}_{\text{prd}}$ is the mean of predicted values.

3 Results and discussion

The most difficult thing in artificial neural network studies is to find the appropriate network architecture, which is based on the determination of the number of optimal layers and neurons in the hidden layers as well as of the suitable activation function. In the present study, three- and four-layer perceptron was investigated by using IBM SPSS version 20 and MATLAB version R2015a software. For MLP-MATLAB, the number of hidden layers was limited to one layer with the sigmoid activation function. The optimal number of neurons was selected using the neural network toolbox. The RBF model was tested for the same version of IBM SPSS. The BP and LM training algorithms were used for IBM SPSS and MATLAB software, respectively. A total of 40 artificial networks were constructed using 99 experimental datasets. For all models, about 70% of samples were randomly assigned to the training phase and the remaining 30% of samples were allocated to the testing phase. The learning and momentum rates were 0.9 and 0.4, respectively. The maximum epoch of the network varied from 1000 to 2000.

The ANN's architectures used in this work are composed of an input layer with six input parameters: percentage of phosphogypsum (PPG), percentage of fly ash (PFA), curing temperature (CT), aging time (AT), sodium hydroxide concentration (SHC) and water (W), one or two hidden layers, and an output layer (compressive strength). The input parameters are the various constituents of the geopolymer specimens as used in the laboratory experiments.

Table 4 lists the fitting values of error functions for single-layer feedforward (RBF) and multilayer perceptron models. Outcomes indicate that the number of neurons in the hidden layers and the activation function affect the performance of the model. Similar observations were reported in the literature [21, 24]. Also from Table 4, we can conclude that the MLP models are able to predict the compressive strength values more accurately than the RBF one. Among multilayer perceptron networks, the MLP-III with architecture 6–8–10–1 (six input neurons, two hidden layers having 8 and 10 neurons, and one output neuron) with the hyperbolic tangent activation function is the best

Table 4 Best-fitting values of the compressive strength of FA–PG-based geopolymer bricks

Models	Hidden layer 1	Hidden layer 2	Activation function	Statistical parameters		
	Number of neurons	Number of neurons		R^2	RMSE	MAE
MLP-I-MATLAB	12	0	Sigmoid	0.9608	0.7320	0.4968
MLP-I-SPSS	16	0	Hyperbolic tangent	0.9434	0.8877	0.6499
MLP-I-SPSS	16	0	Sigmoid	0.8952	1.2398	1.0245
RBF-SPSS	28	0	Gaussian	0.9487	0.8424	0.5963
MLP-II-SPSS	6	8	Hyperbolic tangent	0.9531	0.8037	0.5496
MLP-II-SPSS	6	8	Sigmoid	0.9367	0.9419	0.6861
MLP-III-SPSS	8	10	Hyperbolic tangent	0.9622	0.7185	0.4455
MLP-III-SPSS	8	10	Sigmoid	0.9394	0.9202	0.6742
MLP-IV-SPSS	10	12	Hyperbolic tangent	0.9517	0.8158	0.5576
MLP-IV-SPSS	10	12	Sigmoid	0.9350	0.9551	0.7148

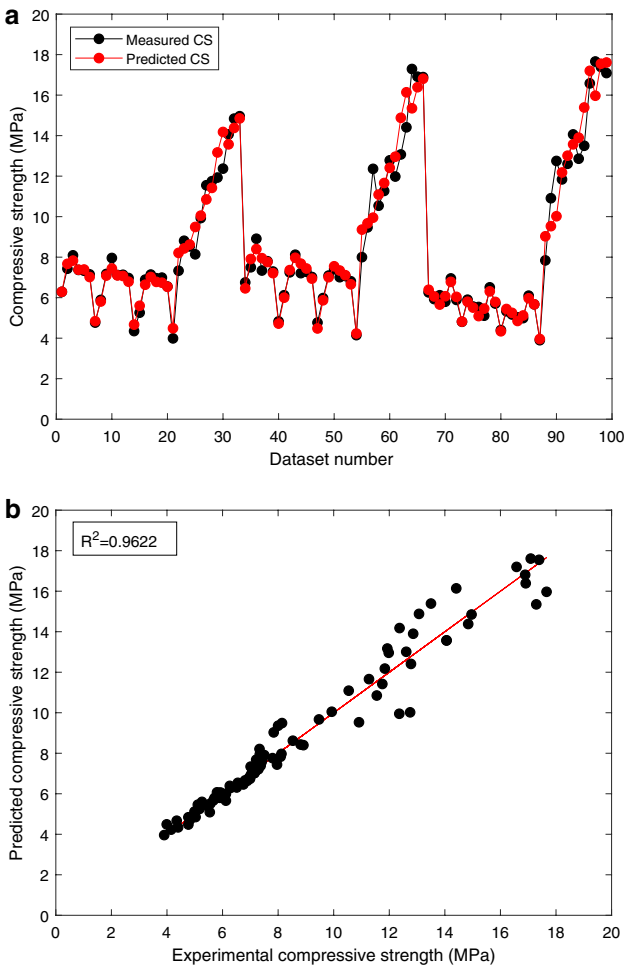

Fig. 3 Predictive performance of the MLP-III (6–8–10–1) model

model for predicting the compressive strength of FA–PG-based geopolymer bricks, as confirmed by its high R^2 value and the lowest RMSE and MAE values. Figure 3a, b depicts the predictive performance of the MLP-III (6–8–10–1) model. From Fig. 3a, it can be seen that the predicted compressive strength values present better agreement with those of experimentally determined values. These results prove that the model was able to reproduce the experimental compressive strength results with high accuracy. The results of the regression analysis (Fig. 3b) show that the experimental and predicted compressive strengths are highly correlated, with a coefficient of determination close to 1.

(a) Comparison between measured and predicted compressive strength values for all samples.
(b) Regression analysis of the MLP-III (6–8–10–1) model.

The reliability of the model was tested for different experimental conditions. The predicted and experimental values of CS, as a function of the percentage of phosphogypsum, for NaOH (1 M), at different curing temperatures and aging times based on MLP-III (6–8–10–1) neural network, are depicted in Fig. 4. The plots indicate that the MLP-III (6–8–10–1) model fits well the experimental data of the compressive strength of FA–PG-based geopolymer bricks. Also from Fig. 4, we can see that by increasing the curing temperature from 60 to 100 °C, the compressive strength decreases from 8.91 to 7.14 MPa. Similar observations were reported in other researches [35, 36]. On the other hand, the rise in aging time beyond 7 days had not a beneficial effect on the compressive strength. In addition, the optimal percentage found of phosphogypsum replacement is 10%. Therefore, the best conditions for Moroccan FA–PG-based geopolymer bricks are 60 °C, 28 days and 10% for curing temperature, aging time and phosphogypsum percentage, respectively.

The effect of sodium hydroxide concentration on the compressive strength, at various aging times, is presented in Fig. 5. The increase in NaOH concentration and aging time leads to the rise in the compressive strength. Indeed, the CS was varied from 8 to 17.4 MPa with the variation of sodium hydroxide from 1 to 15 M. This was ascribed to the formation of sodium aluminosilicate, obtained from the dissolution of Si^{4+} and Al^{3+} ions from fly ash, caused by the increase in NaOH concentration [37].

Figure 6 depicts the relative importance of input parameters on the prediction of the compressive strength of FA–PG geopolymer bricks based on the MLP-III (6–8–10–1) model. The results clearly show that the concentration of sodium hydroxide is the most significant parameter for the compressive strength prediction.

The predictive performance of the MLP-III (6–8–10–1) model was tested on four data from the literature [17, 38–40]. The results are evaluated based on three mathematical error functions: R^2, RMSE and MAE. The obtained values of the fitting error functions are summarized in Table 5. Outcomes indicate that the MLP-III (6–8–10–1) model can fit the experimental data very well.

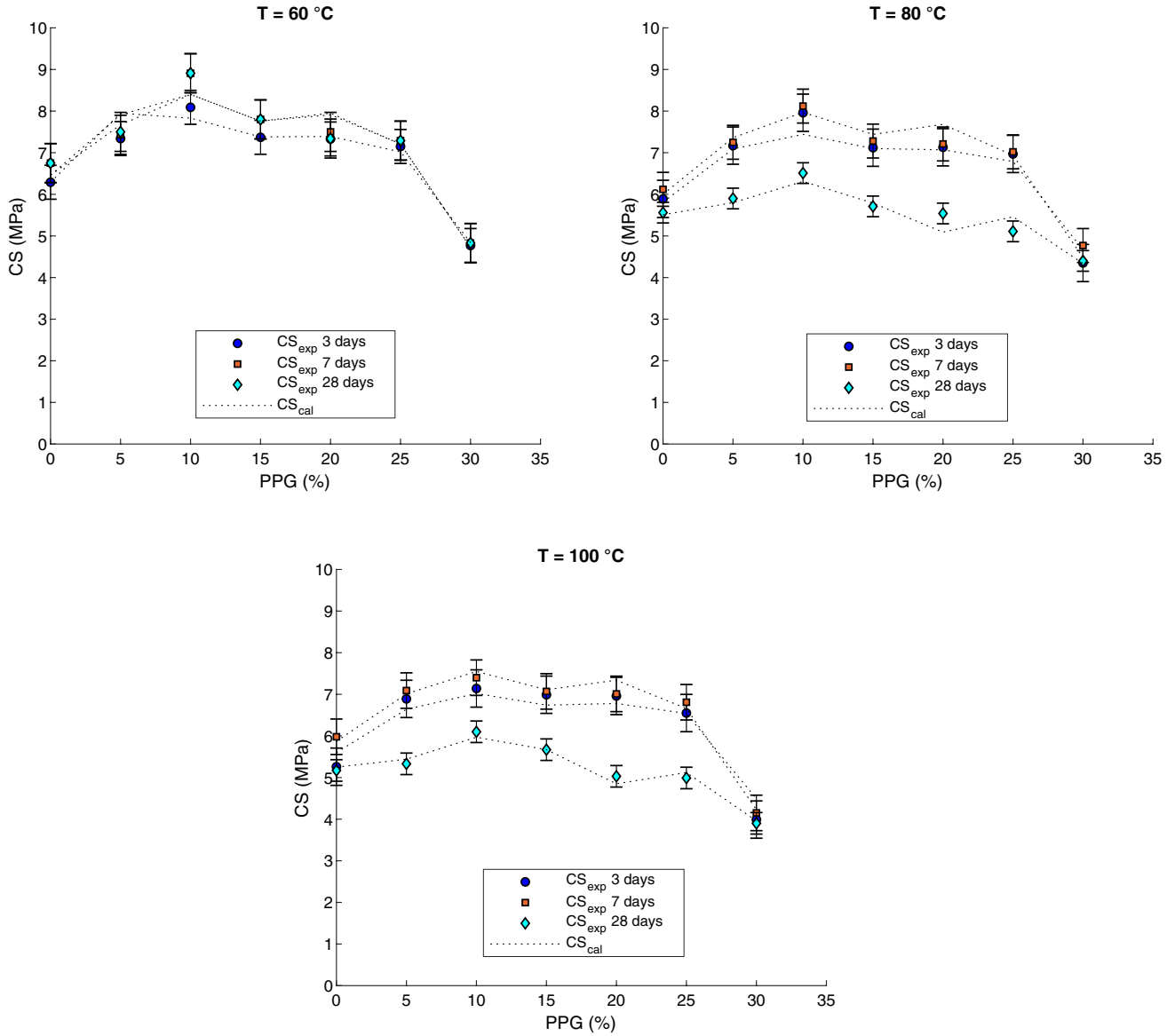

Fig. 4 Compressive strength plots as a function of phosphogypsum percentage, at different curing temperatures and aging times. The symbols and dashed lines are the experimental and predicted values based on MLP-III (6–8–10–1) neural network

4 Conclusion

Fly ash and phosphogypsum can be used as alternate binders for the synthesis of geopolymer bricks. The best geopolymerization process was obtained for 60 °C, 28 days and 10% for curing temperature, aging time and phosphogypsum percentage, respectively.

The artificial neural network was tested as an alternative to experimental tests for simulating the compressive strength of FA–PG-based geopolymers. The results show that the ANN technique may be a promising method for rapid and accurate estimation of the compressive strength of FA–PG-based geopolymer bricks.

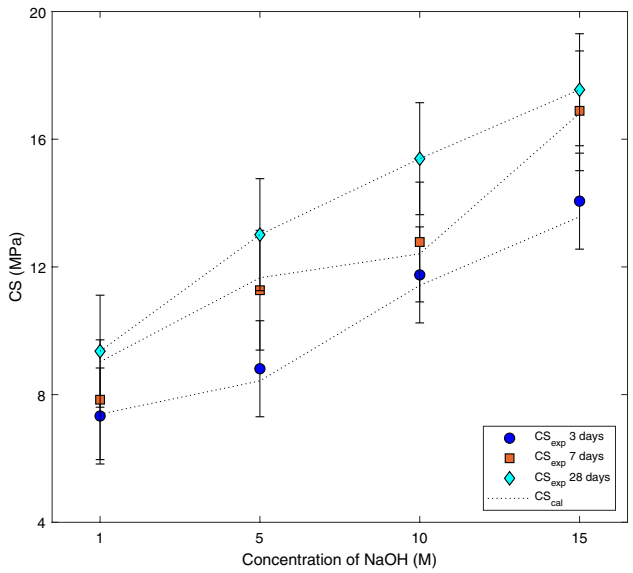

Fig. 5 Effect of NaOH concentration on the compressive strength at various aging times. The symbols and dashed lines are the experimental and predicted values based on MLP-III (6–8–10–1) neural network model

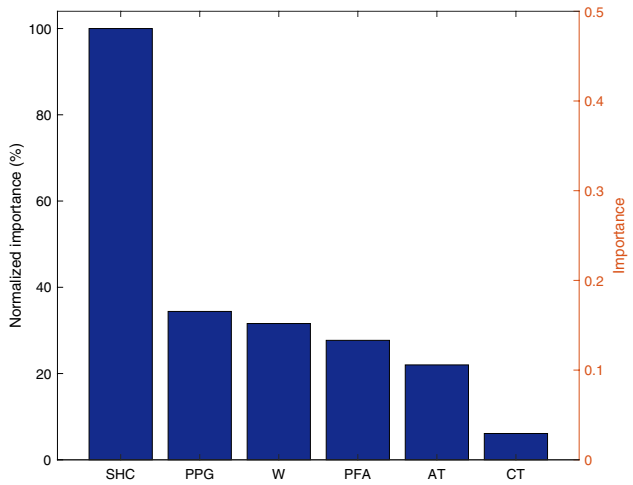

Fig. 6 Relative importance of input parameters for the prediction of the compressive strength of FA–PG geopolymer bricks based on the MLP-III (6–8–10–1) model

Table 5 Fitting error functions values obtained by applying the MLP-III (6–8–10–1) model to data from the literature

	MLP-III (6-8-10-1)		
	R^2	RMSE	MAE
Nazari [17]	0.9903	0.7361	0.3632
Ghezal and Khayat [38]	0.9918	0.7225	0.5644
Nazari and Riahi [39]	0.9806	0.0012	0.00086
Soudki et al. [40]	0.9811	0.9688	0.6848

This study contributes to a better understanding of the synthesis of geopolymer bricks based on fly ash and phosphogypsum and enables the prediction of the compressive strength using the ANN technique.

Compliance with ethical standards

Conflict of interest The authors declare that they have no conflict of interest.

References

1. Altun İA, Sert Y (2004) Utilization of weathered phosphogypsum as set retarder in Portland cement. Cement Concr Compos 34(4):677–680. https://doi.org/10.1016/j.cemconres.2003.10.017
2. Shen W, Zhou M, Zhao Q (2007) Study on lime–fly ash–phosphogypsum binder. Constr Build Mater 21(7):1480–1485. https://doi.org/10.1016/j.conbuildmat.2006.07.010
3. Kumar S (2000) Fly ash-lime-phosphogypsum cementitious binder: a new trend in bricks. Mater Struct 33(1):59–64. https://doi.org/10.1007/BF02481697
4. Shen Y, Qian J, Chai J, Fan Y (2014) Calcium sulphoaluminate cements made with phosphogypsum: production issues and material properties. Cement Concr Compos 48:67–74. https://doi.org/10.1016/j.cemconcomp.2014.01.009
5. Davidovits J (2008) Geopolymer chemistry and applications. Geopolymer Institute, Saint-Quentin
6. Van Jaarsveld JGS, Van Deventer JSJ, Lorenzen L (1997) The potential use of geopolymeric materials to immobilise toxic metals. Part I. Theory and applications. Miner Eng 10:659–669. https://doi.org/10.1016/S0892-6875(98)00121-6
7. Zhu H, Liang G, Zhang Z, Wu Q, Du J (2019) Partial replacement of metakaolin with thermally treated rice husk ash in metakaolin-based geopolymer. Constr Build Mater 221:527–538. https://doi.org/10.1016/j.conbuildmat.2019.06.112
8. Hamdi N, Messaoud IB, Srasra E (2019) Production of geopolymer binders using clay minerals and industrial wastes. C R Chim 22(2–3):220–226. https://doi.org/10.1016/j.crci.2018.11.010
9. Tchadjié LN, Djobo JNY, Ranjbar N, Tchakouté HK, Kenne BBD, Elimbi A, Njopwouo D (2016) Potential of using granite waste as raw material for geopolymer synthesis. Ceram Int 42(2):3046–3055. https://doi.org/10.1016/j.ceramint.2015.10.091
10. Fan F, Liu Z, Xu G, Peng H, Cai CS (2018) Mechanical and thermal properties of fly ash based geopolymers. Constr Build Mater 160:66–81. https://doi.org/10.1016/j.conbuildmat.2017.11.023
11. Embong R, Kusbiantoro A, Shafiq N, Nuruddin MF (2016) Strength and microstructural properties of fly ash based geopolymer concrete containing high-calcium and water-absorptive aggregate. J Clean Prod 112:816–822. https://doi.org/10.1016/j.jclepro.2015.06.058
12. Sata V, Sathonsaowaphak A, Chindaprasirt P (2012) Resistance of lignite bottom ash geopolymer mortar to sulfate and sulfuric acid attack. Cement Concr Compos 34(5):700–708. https://doi.org/10.1016/j.cemconcomp.2012.01.010
13. Yang T, Yao X, Zhang Z (2014) Geopolymer prepared with high-magnesium nickel slag: characterization of properties and microstructure. Constr Build Mater 59:188–194. https://doi.org/10.1016/j.conbuildmat.2014.01.038
14. Zhang Z, Zhu Y, Yang T, Li L, Zhu H, Wang H (2017) Conversion of local industrial wastes into greener cement through geopolymer technology: a case study of high-magnesium nickel

slag. J Clean Prod 141:463–471. https://doi.org/10.1016/j.jclepro.2016.09.147
15. Rashad AM (2015) Potential use of phosphogypsum in alkali-activated fly ash under the effects of elevated temperatures and thermal shock cycles. J Clean Prod 87:717–725. https://doi.org/10.1016/j.jclepro.2014.09.080
16. Rashad AM (2017) Phosphogypsum as a construction material. J Clean Prod 166:732–743. https://doi.org/10.1016/j.jclepro.2017.08.049
17. Nazari A (2013) Compressive strength of geopolymers produced by ordinary Portland cement: application of genetic programming for design. Mater Des 43:356–366. https://doi.org/10.1016/j.matdes.2012.07.012
18. Yuan Z, Wang LN, Ji X (2014) Prediction of concrete compressive strength: research on hybrid models genetic based algorithms and ANFIS. Adv Eng Softw 67:156–163. https://doi.org/10.1016/j.advengsoft.2013.09.004
19. Duan ZH, Kou SC, Poon CS (2013) Using artificial neural networks for predicting the elastic modulus of recycled aggregate concrete. Constr Build Mater 44:524–532. https://doi.org/10.1016/j.conbuildmat.2013.02.064
20. Behnood A, Golafshani EM (2018) Predicting the compressive strength of silica fume concrete using hybrid artificial neural network with multi-objective grey wolves. J Clean Prod 202:54–64. https://doi.org/10.1016/j.jclepro.2018.08.065
21. Eskandari-Naddaf H, Kazemi R (2017) ANN prediction of cement mortar compressive strength, influence of cement strength class. Constr Build Mater 138:1–11. https://doi.org/10.1016/j.conbuildmat.2017.01.132
22. Naderpour H, Mirrashid M (2018) An innovative approach for compressive strength estimation of mortars having calcium inosilicate minerals. J Build Eng 19:205–215. https://doi.org/10.1016/j.jobe.2018.05.012
23. Tenza-Abril AJ, Villacampa Y, Solak AM, Baeza-Brotons F (2018) Prediction and sensitivity analysis of compressive strength in segregated lightweight concrete based on artificial neural network using ultrasonic pulse velocity. Constr Build Mater 189:1173–1183. https://doi.org/10.1016/j.conbuildmat.2018.09.096
24. Nazari A, Torgal FP (2013) Predicting compressive strength of different geopolymers by artificial neural networks. Ceram Int 39(3):2247–2257. https://doi.org/10.1016/j.ceramint.2012.08.070
25. Mansour MY, Dicleli M, Lee JY, Zhang J (2004) Predicting the shear strength of reinforced concrete beams using artificial neural networks. Eng Struct 26(6):781–799. https://doi.org/10.1016/j.engstruct.2004.01.011
26. Naderpour H, Rafiean AH, Fakharian P (2018) Compressive strength prediction of environmentally friendly concrete using artificial neural networks. J Build Eng 16:213–219. https://doi.org/10.1016/j.jobe.2018.01.007
27. Huang GB, Chen L, Siew CK (2006) Universal approximation using incremental constructive feedforward networks with random hidden nodes. IEEE Trans Neural Netw 17:879–892. https://doi.org/10.1109/tnn.2006.875977
28. Haykin SS (2009) Neural networks and learning machines. Pearson Education, Upper Saddle River
29. Harpham C, Dawson CW (2006) The effect of different basis functions on a radial basis function network for time series prediction: a comparative study. Neurocomputing 69:2161–2170. https://doi.org/10.1016/j.neucom.2005.07.010
30. Hornik K, Stinchcombe M, White H (1989) Multilayer feedforward networks are universal approximators. Neural Netw 2:359–366. https://doi.org/10.1016/0893-6080(89)90020-8
31. Gardner MW, Dorling S (1998) Artificial neural networks (the multilayer perceptron) a review of applications in the atmospheric sciences. Atmos Environ 32:2627–2636. https://doi.org/10.1016/S1352-2310(97)00447-0
32. Karimi R, Yousefi F, Ghaedi M, Dashtian K (2016) Back propagation artificial neural network and central composite design modeling of operational parameter impact for sunset yellow and azur (II) adsorption onto MWCNT and MWCNT-Pd-NPs: isotherm and kinetic study. Chemom Intell Lab Syst 159:127–137. https://doi.org/10.1016/j.chemolab.2016.10.012
33. El Boundati Y, Ziat K, Naji A, Saidi M (2019) Generalized fractal-like adsorption kinetic models: application to adsorption of copper on Argan nut shell. J Mol Liq 276:15–26. https://doi.org/10.1016/j.molliq.2018.11.121
34. Getahun MA, Shitote SM, Gariy ZCA (2018) Artificial neural network based modelling approach for strength prediction of concrete incorporating agricultural and construction wastes. Constr Build Mater 190:517–525. https://doi.org/10.1016/j.conbuildmat.2018.09.097
35. Salih MA, Farzadnia N, Ali AAA, Demirboga R (2015) Effect of different curing temperatures on alkali activated palm oil fuel ash paste. Constr Build Mater 94:116–125. https://doi.org/10.1016/j.conbuildmat.2015.06.052
36. Muñiz-Villarreal MS, Manzano-Ramírez A, Sampieri-Bulbarela S, Gasca-Tirado JR, Reyes-Araiza JL, Rubio-Ávalos JC, Perez Bueno J, Apatiga LM, Zaldivar-Cadena A, Amigó-Borrás V (2011) The effect of temperature on the geopolymerization process of a metakaolin-based geopolymer. Mater Lett 65(6):995–998. https://doi.org/10.1016/j.matlet.2010.12.049
37. Hanjitsuwan S, Hunpratub S, Thongbai P, Maensiri S, Sata V, Chindaprasirt P (2014) Effects of NaOH concentrations on physical and electrical properties of high calcium fly ash geopolymer paste. Cement Concr Compos 45:9–14. https://doi.org/10.1016/j.cemconcomp.2013.09.012
38. Ghezal A, Khayat KH (2002) Optimizing self-consolidating concrete with limestone filler by using statistical factorial design methods. ACI Mater J 99(3):264–272
39. Nazari A, Riahi S (2013) Artificial neural networks to prediction total specific pore volume of geopolymers produced from waste ashes. Neural Comput Appl 22(3–4):719–729. https://doi.org/10.1007/s00521-011-0760-x
40. Soudki KA, El-Salakawy EF, Elkum NB (2001) Full factorial optimization of concrete mix design for hot climates. J Mater Civ Eng 13(6):427–433. https://doi.org/10.1061/(ASCE)0899-1561(2001)13:6(427)